Journal of
Applied Crystallography

ISSN 0021-8898

Received 6 September 2007
Accepted 30 April 2008

Application of small-angle scattering to study the effects of moisture content on a native soy protein

Catherine S. Kealley,[a]* Margaret M. Elcombe,[a] Richard Wuhrer[b] and Elliot P. Gilbert[a]

[a]Bragg Institute, Australian Nuclear Science and Technology Organization, PMB 1, Menai, NSW, Australia, and [b]Microstructural Analysis Unit, University of Technology, Sydney, PO Box 123, Broadway, NSW, Australia. Correspondence e-mail: catherine.kealley@uts.edu.au

The nano- and microstructure of glycinin, a soybean protein, has been investigated as a function of moisture for moisture contents between 4 and 21 wt%. Glycinin exhibits peaks in the small-angle region whose positions show minimal change with X-rays for samples up to 13% moisture. However, the use of neutron scattering, and the associated enhancement in contrast, results in the Bragg peaks being well resolved up to higher moisture contents; the associated shift in peak positions between 4 and 21% moisture are consistent with the expansion of a hexagonal unit cell as a function of moisture content. A Porod slope of ~ -4 indicates that the interface between the 'dry' protein powder and the surrounding medium at a length-scale of at least 3 μm down to ~20 nm is smooth and sharp. Scanning electron microscopy indicates that the powders, with low moisture content, have a porous appearance, with the porosity decreasing and microstructure expanding as the moisture content increases.

1. Introduction

Nature rarely produces proteins in a concentrated or dry state, with the exception of proteins as energy storage reserves in seeds. Proteins are more commonly found in heavily hydrated cellular systems, where their unique folded conformations are active as biocatalysts (enzymes), recognition systems (antibodies), flexible ordered structures (muscle tissue, connective tissue) and nutrient carriers (milk). When proteins are dried for reasons of storage stability, the subsequently rehydrated forms do not exhibit the same properties as the original native states (Aguilera & Stanley, 1999). Proteins exhibit nonlinear behaviour during water loss to the dried state. In particular, hysteresis in water-sorption curves is usually observed, implying kinetic control of events at low moisture content. This almost certainly relates to the formation of metastable glasses in which very slow conformational change occurs (Aguilera & Stanley, 1999).

Soybean proteins are used in foods as gelling, emulsifying and foaming agents (Utsumi *et al.*, 1997). Soybean proteins are composed of two major components, glycinin (11S globulin) and β-conglycinin (7S globulin), which account for about 40 and 30% of the total seed proteins, respectively. Glycinin extracted from seeds is a hexameric protein with a molecular mass of 300–380 kDa (Adachi *et al.*, 2001). Each subunit is composed of an acidic (~32 kDa) and a basic (~20 kDa) polypeptide linked by a disulfide bond (Staswick *et al.*, 1984). Constituent subunits of glycinin have two or three disulfide bonds, and the five major subunits of glycinin have been identified as A1aB1b, A2B1a, A1bB2, A3B4 and A5A4B3 (Utsumi *et al.*, 1997; Adachi *et al.*, 2001). Six subunits form a hexamer, and there are three hexamers in a unit cell. The A3B4 homohexamer of glycinin has the space group $R3$, with cell dimensions $a = 11.484$, $b = 11.484$, $c = 19.157$ nm with $\alpha = \beta = 90^\circ$ and $\gamma = 120^\circ$ in the hexagonal obverse setting (Adachi *et al.*, 2003).

The work reported here will centre on the structure of native glycinin, *i.e.* the non-homohexameric protein, at low and controlled moisture content. Small-angle neutron and X-ray scattering have been used to monitor changes in the unit-cell dimensions, and scanning electron microscopy has been used to follow changes in the microstructure of the protein powder as the moisture content is increased. By determining the structure and behaviour of such food-relevant proteins, it becomes possible to identify and develop design criteria for the properties of proteins in relation to dried foods and ingredients.

2. Experimental

2.1. Materials

Defatted soy flour was initially obtained from Archer Daniels Midland Company (ADM), Illinois, USA. Soy glycinin was extracted from the flour following a modification of the protocol of Bogracheva *et al.* (1996). In brief, the flour was stirred with water in a 1:7 ratio, and the pH of the suspension was adjusted to 8.0 by slowly adding 1 *M* NaOH. The suspension was further stirred at room temperature for 30 min, followed by centrifugation at 6000 r min^{-1} for 20 min

at room temperature. The supernatant was adjusted to pH 6.8 using 1 *M* HCl and incubated at 277 K for 16 h without stirring. The bottom phase was washed twice briefly with Milli-Q water and freeze dried. Hydration was achieved by leaving the material in sealed containers with saturated salt solutions. Humidity levels were measured by mass change on drying by thermogravimetric analysis.

The protein content of soy glycinin (11S) was determined to be 96.3% by the micro-Kjeldahl method (Concon & Soltess, 1973) using a nitrogen-to-protein conversion factor of 6.2. The purity and homogeneity of glycinin were checked by sodium dodecyl sulfate polyacrylamide gel electrophoresis (Agilent Lab-on-a-chip equipment) following the manufacturer's instructions. All chemicals used were of analytical grade.

2.2. Small-angle X-ray scattering

Native glycinin powders with increasing moisture content (4.6, 6.2, 9.2, 11.4, 13.4 and 17.1%) were loaded into 2 mm quartz capillaries for the collection of small-angle X-ray scattering (SAXS) data. SAXS measurements were performed on a Bruker Nanostar SAXS camera with pin-hole collimation for point focus geometry. The instrument source is a copper rotating anode (0.3 mm filament) operating at 45 kV and 110 mA, fitted with cross-coupled Göbel mirrors, resulting in Cu $K\alpha$ radiation (wavelength 0.154 nm). The SAXS camera is fitted with a Hi-star two-dimensional detector (effective pixel size 100 µm). The optics and the sample chamber were evacuated to minimize air scatter. A short- (250 mm) and a mid-range (658 mm) sample-to-detector distance were used, giving a q range of 0.5–8.0 nm^{-1}; q is the magnitude of the scattering vector, defined as $q = (4\pi/\lambda)\sin\theta$, where λ is the wavelength and 2θ is the scattering angle. Scattering files were normalized to sample transmission, background subtracted and then radially averaged using *Nika* (Ilavsky, 2006) software.

2.3. Ultra-small-angle X-ray scattering

Ultra-small-angle X-ray scattering (USAXS) experiments were conducted on the USAXS instrument installed at beamline 33ID (XOR-UNI) at the Advanced Photon Source, Argonne National Laboratory, USA. The monochromator was set to 10.99 keV (0.113 nm), generating about 10^{13} photons s^{-1} incident on the sample in an area approximately 2 mm wide and 0.5 mm high. The instrument uses a photodiode detector with approximately nine orders of magnitude of intensity range between the direct beam and instrument background. USAXS data were collected for q values from 0.0015 to 0.50 nm^{-1}. For these measurements the instrument was assembled in slit geometry. Slit-smeared data were processed with the code developed for use on this USAXS instrument, including numerical desmearing of the USAXS data using the Lake (1967) method as implemented by Long *et al.* (1991).

2.4. Small-angle neutron scattering

Native glycinin powders of two moisture contents (~6 and ~17%) were recrystallized from D_2O solutions and then hydrated from salt solutions with different amounts of D_2O (0, 20, 40, 60, 80 and 100%). These samples were then studied using small-angle neutron scattering (SANS) to monitor the effect of the water on the structure of the protein. The SANS data were collected on the Australian Small Angle Neutron Scattering Facility (AUSANS). The q range over which data were collected is 0.1–1.0 nm^{-1}, at a wavelength of 0.35 nm. The samples were contained in ~2 mm cuvettes and the collection time was 8 h per sample.

2.5. Scanning electron microscopy

Scanning electron microscopy was performed with a Philips (FEI) XL30 Environmental Scanning Electron Microscope (ESEM). An ESEM allows the examination of surfaces of almost any specimen (wet or dry) as the environment around the specimen does not have to be at a high vacuum. A differential pumping system is used to maintain the electron gun at high vacuum, while the air at atmospheric pressure in the chamber is replaced by water vapour at a few torr (Goldstein *et al.*, 2003). The ESEM, operating in low-vacuum mode, was used for low-magnification images of uncoated native glycinin powder samples with the water vapour pressure selected as close to the samples' moisture content as possible. Real-time hydration/dehydration studies were then carried out, with the water condensing onto or evaporating from the sample, to dynamically monitor any changes in the samples.

3. Results and discussion

To provide information from the nano- to micrometre scale, USAXS, SAXS and SANS techniques were used in this work, measuring over four orders of magnitude in length-scale. The SAXS and SANS data collected from native glycinin are shown in Fig. 1. In general, a decrease in the intensity of the SAXS data is observed as the moisture content (MC) increases; this is associated with a reduction in scattering

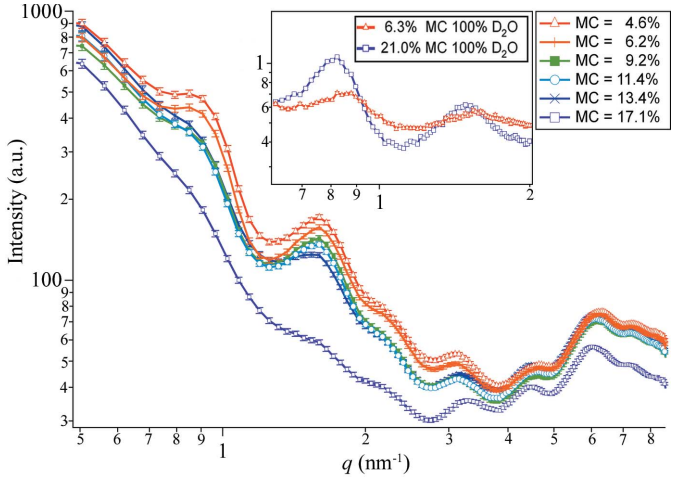

Figure 1
Small-angle X-ray scattering data from glycinin with increasing moisture content. The inset is a selected region from the small-angle neutron scattering data with H_2O replaced by D_2O at two moisture contents.

Table 1
X-ray and neutron scattering length densities of H_2O, D_2O and proteins (Svergun & Koch, 2003).

	X-rays ($\times 10^{10}$ cm^{-2})	Neutrons ($\times 10^{10}$ cm^{-2})
H_2O	9.46	−0.56
D_2O	9.46	6.34
Proteins (H)	11.84	1.8–3.1
Proteins (D)	11.84	6.6–8.0

Table 2
Power-law exponents from fitting the Porod region in USAXS data.

Moisture content	Slope
4.6%	−4.03 (1)
6.2%	−3.98 (1)
9.2%	−3.95 (2)
11.4%	−4.17 (2)
13.4%	−4.09 (1)
17.1%	−4.08 (1)

Table 3
Effect of increasing moisture content on the unit-cell parameters of glycinin.

The values in parentheses correspond to the uncertainty in the least significant figures. The goodness-of-fit (χ^2) is shown for each data set.

% MC	a (nm)	c (nm)	Volume (nm^3)	χ^2
4.6	9.63 (6)	18.2 (1)	1460 (28)	1.724
6.2	9.64 (7)	18.2 (1)	1466 (27)	1.696
9.2	9.64 (7)	18.3 (1)	1472 (33)	1.947
11.4	9.64 (7)	18.3 (1)	1475 (34)	2.260
13.4	9.6 (1)	18.4 (3)	1482 (155)	3.527

contrast. At low moisture content, the scattering contrast arises primarily from the scattering length density difference of the protein relative to air; as moisture is added, the scattering is more complicated and is associated with three scattering length densities, namely protein, water and air, and therefore three contrasts. As shown in Table 1, both the protein and water have a high scattering length density for X-rays, so, as water replaces air in the system, the overall contrast is lowered, thus reducing the scattering intensity. The use of D_2O substitution for the SANS experiments enables improved contrast at the higher moisture contents and lowers the contribution from incoherent background scattering (see Fig. 1 inset).

Gaussian functions associated with seven peaks (see Fig. 2) were simultaneously fitted to the SAXS peaks to determine the peak characteristics. In order to improve the resolution of the data, a longer camera length (658 mm) was used, hence the q range fitted in Fig. 2 is 0.3–3.0 nm^{-1}. Removal of any of the seven peaks leads to a significant decrease in the goodness-of-fit and increases the errors on the remaining peak positions. The baseline was fitted by a power-law $y = Aq^{-P} + C$ function, where A and C are constants, based on the results from the fitting of the USAXS data (see Table 2).

It is possible to use the peak positions to determine $1/d^2$, where d simply represents the associated real-space dimension, and then identify possible unit-cell symmetries for the crystal structure of the native glycinin. Adachi *et al.* (2003) isolated the A3B4 subunit and hence reported a crystal structure for a homohexamer of glycinin. Adachi *et al.* (2003) have shown that there are three hexamers in the hexagonal unit cell of glycinin with dimensions of $a = b = 11.484$, $c = 19.157$ nm, and a volume of 2188 nm^3. After fitting (results shown in Table 3), the experimental SAXS data were found to be consistent with a hexagonal unit cell. As the moisture content increases, the peaks become less defined and the broadening of the lines of the less resolved peaks results in larger errors. The poor peak resolution is inherent to these samples. It is not possible to determine the unit-cell parameters from the 17.1% moisture content sample because the peaks are less distinct (see Fig. 1) as a result of the lower contrast. Although a cursory glance at the data would appear to show that, in general, the Bragg peaks shift to lower q with increasing moisture content, the intrinsic uncertainty in peak positions and therefore unit-cell parameters precludes such a definitive conclusion. Overall, the experimental data show that the unit cell of native glycinin (a combination of all subunits) is smaller than the Adachi *et al.* (2003) homohexamer, the latter comprising only one subunit (A3B4).

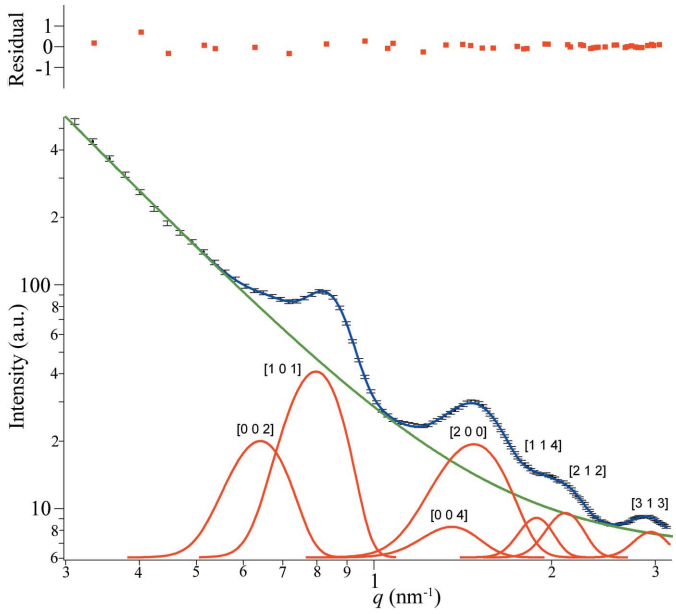

Figure 2
Gaussian fitting of the small-angle X-ray scattering data collected from the 4.6% MC glycinin sample. The black dots are the data, the blue line is the fit, the green line is the background, and the red dots represent the residual difference pattern. The Gaussian peaks and their respective indices are shown.

The SANS data show a similar peak shift to lower q (higher d spacing) with increasing moisture content, apparently expanding the unit cell, as can be seen by a comparison of the peak positions in the inset of Fig. 1. Using the known reflections from the SAXS data, it was possible to index the two peaks in the neutron data to give an overall expansion of about 15% of the unit cell from 6.3 to 21.0% MC. The expansion is more obvious in the neutron data than in the SAXS data, as the samples hydrated with D_2O exhibit greater

Table 4
FWHM values determined from the Gaussian fits of the SAXS data.

The values in parentheses correspond to the uncertainty in the least significant figures.

4.6% MC		6.2% MC		9.2% MC		11.4% MC		13.4% MC	
q	FWHM	q	FWHM	q	FWHM	q	FWHM	q	FWHM
0.676 (5)	0.088 (1)	0.685 (5)	0.106 (2)	0.688 (5)	0.122 (2)	0.689 (5)	0.126 (6)	0.690 (5)	0.113 (7)
0.832 (1)	0.097 (3)	0.830 (1)	0.096 (1)	0.825 (2)	0.087 (2)	0.821 (2)	0.083 (2)	0.819 (2)	0.080 (3)
1.383 (3)	0.193 (4)	1.380 (4)	0.195 (5)	1.365 (3)	0.225 (6)	1.369 (5)	0.223 (3)	1.371 (5)	0.220 (8)
1.502 (2)	0.232 (4)	1.501 (2)	0.231 (2)	1.501 (2)	0.227 (2)	1.500 (2)	0.224 (3)	1.500 (2)	0.225 (3)
1.899 (4)	0.156 (6)	1.894 (3)	0.163 (5)	1.897 (4)	0.170 (5)	1.894 (4)	0.170 (5)	1.890 (4)	0.173 (6)
2.116 (3)	0.185 (1)	2.116 (3)	0.194 (4)	2.111 (3)	0.183 (4)	2.110 (3)	0.185 (5)	2.111 (4)	0.192 (5)
2.912 (4)	0.242 (4)	2.901 (5)	0.231 (4)	2.926 (6)	0.259 (9)	2.949 (6)	0.28 (1)	2.973 (7)	0.29 (1)

contrast, allowing the analysis of data from samples with higher moisture content (21%) as the peaks are well resolved. Conversely, lower contrast, less resolved peaks are obtained for the 13% moisture content SAXS samples.

The glass transition temperature (T_g) is defined as the temperature at which the thermal expansion coefficient undergoes a discontinuity. Below T_g configurational rearrangements of polymer chain backbones are extremely slow (Ferry, 1980). Water acts as a plasticizing agent and, as the moisture content increases, T_g decreases. There exists a corresponding moisture content at which T_g is numerically equal to ambient temperature. Samples with moisture content below this level are nominally glass-like at ambient temperatures, while those above are nominally 'rubber-like', although the demarcation is far from sharp. For this system, the midpoint T_g is at ambient temperature for a moisture content of around 13%, although the onset of the transition occurs as much as 293 K below this (Rout & Appelqvist, 2007).

There is little change in the full width at half-maximum (FWHM) of the SAXS Bragg reflections with increasing moisture content (see Table 4), suggesting a minimal change in the long-range order of the sample. The exception is the sample with 17.1% MC, where there is an apparent broadening of the peaks. While this is consistent with the moisture content being sufficiently high as to result in the protein being above its glass transition at ambient temperature, the feature is more likely attributed to a further loss in contrast in the scattering relative to the lower-MC samples. Indeed, this observation is further strengthened when compared with the higher-moisture sample in the neutron data.

The SAXS intensity for glassy systems has been shown to increase with temperature and exhibit a discontinuity at T_g (Duiser & Keijzers, 1978). In the current study, the moisture content and not the temperature has been varied. As mentioned earlier, there is a general trend for the intensity to decrease with moisture content, except in the region between $q = 0.5$ and 1.0 nm^{-1}. In this case, the intensity decreases until a moisture content of 9.2% and then plateaus for the 11.4 and 13.4% samples, before decreasing further at 17.1% (Fig. 1). This feature may indicate that the initial stage of the glass transition is occurring in the native glycinin around a moisture content of 11.4%.

The scattering in Fig. 1 arises from a combination of Bragg diffraction from the glycinin crystal structure and the interface between the protein and the surrounding medium. The latter is responsible for the high scattering (Porod scattering) in the low-q region. USAXS (Fig. 3) shows a clear Porod region and, for $q < 0.3$ nm^{-1}, yields power-law exponents as shown in Table 2. This power of ~ -4 indicates that the interface between the protein and the surrounding medium at a length-scale of at least 3 µm down to ~20 nm is smooth and sharp. There is a discontinuity in the slope at 11.4% that once again may be associated with the onset of the glass transition.

The SANS data in Fig. 4 have been fitted with a combination of a power-law ($y = Aq^{-P}$) and two Gaussian peaks, and the refined parameters are given in Table 5. While the power-law slopes differ between SAXS and SANS for corresponding

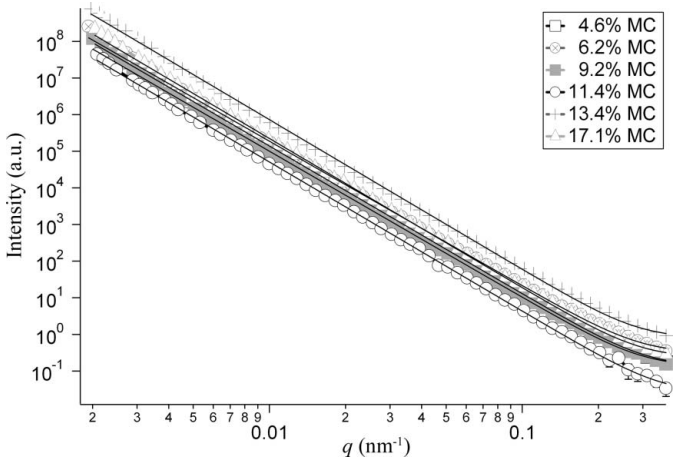

Figure 3
Ultra-small-angle X-ray scattering data collected from glycinin with increasing moisture content (MC) and associated power law fits.

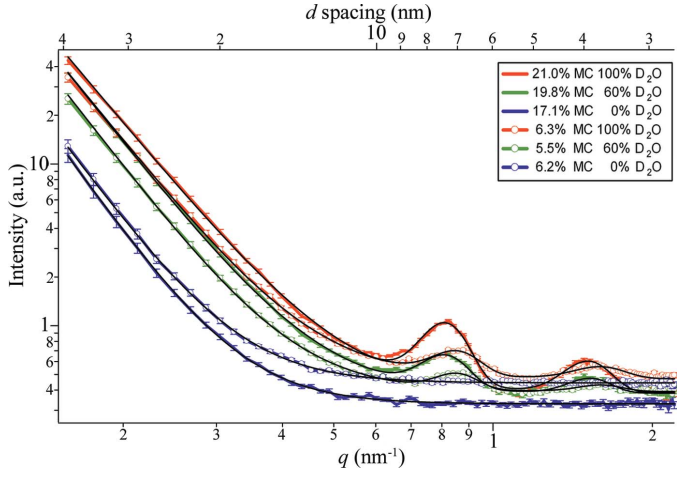

Figure 4
SANS data from the low- and high-MC samples for different H_2O/D_2O compositions, with fits to a combined power law and two Gaussian peak function.

Table 5
The exponent from a combined power law and double Gaussian fit of the low and high moisture content SANS data.

Sample	Low MC	High MC
0% D_2O	-4.46 ± 0.06	-4.62 ± 0.07
20% D_2O	-4.36 ± 0.05	-4.50 ± 0.05
40% D_2O	-4.29 ± 0.06	-4.29 ± 0.04
60% D_2O	-4.27 ± 0.04	-4.14 ± 0.03
80% D_2O	-4.17 ± 0.04	-3.97 ± 0.03
100% D_2O	-4.07 ± 0.03	-3.94 ± 0.02

moisture content samples, we note that the q range over which a power law may be fitted is significantly less than that available using USAXS. Nonetheless, this is likely to be less significant than the inherent interfacial contrast differences between the two sources of radiation (*i.e.* neutrons and X-rays are sensitive to different features of the system). Indeed, we cannot rule out the possibility that H_2O and D_2O are not uniformly distributed in these hydrated samples, giving rise to potentially even more complex variations in interfacial scattering. We have not sought to model the location of water in this complex system. Since we observe intensity changes in the Bragg reflections with contrast, the water must be at least partly located on the size range of the individual protein units and preferentially associated with the hydrophilic regions. A more detailed assessment of water location is not possible with the available data, but more information could be obtained using inelastic neutron scattering.

There is a steady decrease in the power-law exponent as the D_2O substitution is increased in both the low- and the high-MC samples, *i.e.* no contrast match point. This results from the effective three-phase nature of the system (protein, water and air). However, note that at 40% D_2O the Porod slope is invariant with moisture content (Table 5). This solvent composition has a scattering length density comparable to that anticipated for the protein (Table 1). As the D_2O content in the system increases either *via* moisture content or by molar composition of the solvent, higher-amplitude peaks are observed as a result of changes in the structure factors of the associated reflections and a decrease in the incoherent background scattering (Fig. 4).

The expansion of the glycinin structure as the moisture content is increased is also seen on the microscopic scale. A hydration/dehydration study was conducted using ESEM (Fig. 5). The sample with a moisture content of 17.1% started

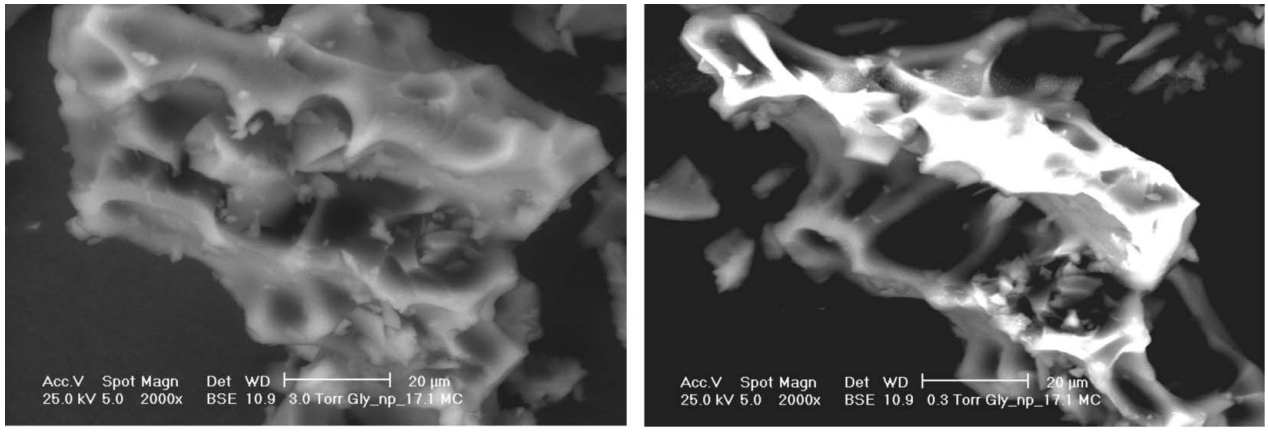

(*a*) (*b*)

Figure 5
ESEM micrographs of the *in situ* drying of a powder particle of native glycinin at (*a*) 3.0 torr (~18% relative humidity) and (*b*) 0.3 torr (< 2% relative humidity).

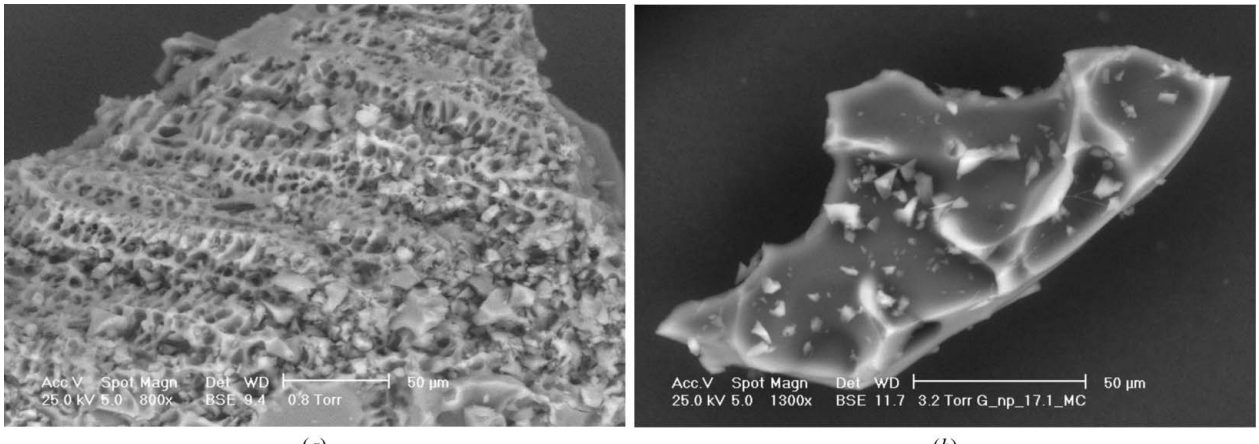

(*a*) (*b*)

Figure 6
ESEM micrographs of (*a*) the 4.6% and (*b*) the 17.1% moisture content powder samples of glycinin.

at its original water vapour pressure of 3.0 torr (∼17% relative humidity) and, when the water vapour pressure was decreased (chamber reached 0.3 torr), the width of the particle visibly shrank by about 20%. The lack of water vapour in the atmosphere has also resulted in the edge-highlighting appearing from the uncoated sample. When the chamber was switched back to 3.0 torr, the protein particle shown immediately began to expand, almost returning to its original size. It should be noted that there was some beam damage but this is considered to be relatively minor.

Fig. 6 shows ESEM micrographs from the 4.6% native glycinin in a 0.8 torr environment (∼5% relative humidity) and the 17.1% native glycinin in a 3.2 torr environment (∼18% relative humidity). The physical appearance of the particles is observed to change with increasing moisture content. The low-MC (4.6%) sample has particles that appear porous. As the moisture content is increased, the material becomes visually less porous and more slate-like.

4. Concluding remarks

We have monitored the structural changes in glycinin over four orders of magnitude of length-scale using a combination of USAXS, SAXS, SANS and ESEM. USAXS shows that the protein-bulk (water, air) interface at a length-scale of at least 3 μm down to ∼20 nm is smooth and sharp. Both SAXS and SANS appear to indicate that the hexagonal unit cell of the protein expands as the moisture content increases. Scanning electron microscopy also indicates that, as the moisture content of the protein powder is increased, the structure expands on the micrometre size scale. In subsequent studies we will investigate the influence of moisture content on both the protein and the water dynamics.

This work was carried out in collaboration with the CSIRO Food Futures Flagship, Food Science Australia and the University of Queensland. The authors would like to acknowledge Mr Aung Htoon, Dr Manoj Rout and the team at Food Science Australia for providing the dry glycinin powders. Acknowledgements also to instrument scientists Dr Tracey Hanley (SAXS – ANSTO), Dr Robert Knott (SANS – ANSTO) and Dr Jan Ilavsky (USAXS – APS). Use of the Advanced Photon Source was supported by the US Department of Energy, Office of Science, Office of Basic Energy Sciences, under contract No. DE-AC02-06CH11357.

References

Adachi, M., Kanamori, J., Masuda, T., Yagasaki, K., Kitamura, K., Mikami, B. & Utsumi, S. (2003). *Proc. Natl Acad. Sci. USA*, **100**, 7395–7400.

Adachi, M., Takenaka, Y., Gidamis, A. B., Mikamu, B. & Utsumi, S. (2001). *J. Mol. Biol.* **305**, 291–305.

Aguilera, J. M. & Stanley, D. W. (1999). *Microstructural Principles of Food Processing and Engineering*, 2nd ed. Gaithersburg: Aspen Publishers.

Bogracheva, T. Y., Bespalova, N. Y. & Leontev, A. L. (1996). *Appl. Biochem. Microbiol.* **32**, 429–433.

Concon, J. M. & Soltess, D. (1973). *Anal. Biochem.* **53**, 35–41.

Duiser, J. A. & Keijzers, A. E. M. (1978). *Polymer*, **19**, 889–894.

Ferry, J. D. (1980). *Viscoelastic Properties of Polymers*, 3rd ed., pp. 280–285. New York: John Wiley and Sons.

Goldstein, J., Newbury, D., Joy, D., Lyman, C., Echlin, P., Lifshin, E., Sawyer, L. & Michael, J. (2003). *Scanning Electron Microscopy and Microanalysis*, 3rd ed. New York: Kulwer Academic/Plenum Publishers.

Ilavsky, J. (2006). *Nika: Package of Two-Dimensional–One-Dimensional SAS Data Reduction Macros for Igor Pro*. Advanced Photon Source, Chicago, USA.

Lake, J. A. (1967). *Acta Cryst.* **23**, 191–194.

Long, G. G., Jemian, P. R., Weertman, J. R., Black, D. R., Burdette, H. E. & Spal, R. J. (1991). *J. Appl. Cryst.* **24**, 30–37.

Rout, M. K. & Appelqvist, I. A. M. (2007). Unpublished data.

Staswick, P. E., Hermodson, M. A. & Nielsen, N. C. (1984). *J. Biol. Chem.* **259**, 13431–13435.

Svergun, D. I. & Koch, M. H. J. (2003). *Rep. Prog. Phys.* **66**, 1735–1782.

Utsumi, S., Matsumura, Y. & Mori, T. (1997). *Structure–Function Relationships of Soy Proteins*, in *Food Proteins and Their Applications*, edited by S. Damodaran & A. Paraf, pp. 257–291. New York: Marcel Dekker.